

Macroscopic magnetization of primordial plasma by virial shocks

Uri Keshet¹ and Kuan-Chou Hou²

¹ Physics Department, Ben-Gurion University of the Negev, POB 653, Be'er-Sheva 84105, Israel; keshet.uri@gmail.com

² Institute of Astronomy and Astrophysics, Academia Sinica, PO Box 23-141, Taipei 10617, Taiwan

Abstract

Galaxy-cluster virial (structure-formation accretion) shock observations are shown to imply $\gtrsim 1\%$ magnetization of a layer extending $\gtrsim 10^{16}$ Debye lengths downstream, challenging the modelling of high Alfvén-Mach collisionless shocks. Unlike similar shocks in supernova remnants or relativistic shocks in γ -ray burst afterglows, where macroscopic magnetized layers were detected but purportedly attributed to preexisting or non-resonant cosmic-ray streaming-seeded substructure, the upstream of strong virial shocks is both weakly magnetized and pristine. Hence, some mechanism must generate large-scale and possibly self-similar magnetic sub-structure out of the accreted primordial plasma; such a mechanism may dominate other high-Mach shock systems, too.

1. Introduction

Collisionless shocks, central to astrophysics as tracers of fast flows and as sources of cosmic-rays (CRs) and seed magnetic fields, are still not understood from first principles, despite decades of research (for reviews, see [Treumann, 2009](#); [Bykov and Treumann, 2011](#); [Sironi et al., 2015](#); [Vanthieghem et al., 2020](#)). CRs are generally understood to arise from first-order Fermi, so-called diffusive shock acceleration, and several mechanisms for shock magnetization were identified. However, in the absence of a self-consistent model for the non-linear, multi-scale, three-dimensional shock structure, it is not possible at present to compute macroscopic shock properties of interest, such as the fractional energies deposited in magnetic fields and in different particle species, or the configuration and extent of the shock-magnetized region. Such parameters are directly needed for modeling the radiative and CR output of the shock, and are indirectly important for understanding the energetics, stability, and various other properties of the host system.

The magnetic-field structure, in particular, determines the synchrotron emission from the shock and its polarization, and affects the subsequent evolution of the plasma and even the energy spectra of CRs and their radiative signature. Notably, although the CR spectrum is thought to be independent of magnetic-field details for non-relativistic shocks ([Krymskii, 1977](#); [Axford et al., 1977](#); [Bell, 1978](#); [Blandford and Ostriker, 1978](#)), provided that the magnetic structure is frozen in the fluid frame and scattering is sufficiently isotropic ([Keshet et al., 2020a](#)), this is no longer true for relativistic shocks ([Kirk et al., 2000](#); [Keshet and Waxman, 2005](#)) in systems of more than one dimension ([Keshet, 2017](#); [Lavi et al., 2020](#)), where anisotropic fields can lead to extreme spectra ([Arad et al., 2021](#)). More importantly for the present study, the microscopically vast extents of the magnetized layers inferred from observations downstream of shocks impose a considerable challenge for collisionless shock modelling.

In supernova remnants (SNRs), extended near-equipartition magnetic fields B are inferred downstream of the shock, although the far upstream field B_u is dynamically insignificant, with a typical magnetic-to-kinetic energy fraction $\sigma \equiv M_A^{-2} = B_u^2 / (4\pi n_u \bar{m} v_u^2) \simeq 10^{-4}$. Here, n_u and v_u are the upstream rest-frame number density and shock velocity, M_A is the Alfvénic Mach number, and \bar{m} is the mean particle mass. In particular, high-resolution X-ray observations imply $B/B_u \simeq 10\text{--}50$, with such elevated B values persisting $\gtrsim 10^{17}$ cm downstream of the shock ([Vink and Laming, 2003](#); [Bamba et al., 2003](#); [Völk et al., 2005](#); [Ressler et al., 2014](#); [Vink, 2020](#)). Hence, strongly magnetized substructure must be seeded near the shock and survive extremely far (in microscopic terms) downstream, over $\gtrsim 10^{12} l_D$ Debye lengths or $\gtrsim 10^9 r_L(B)$ Larmor radii. These scales vastly exceed the shock width and natural scales of thermal plasma instabilities, implying an additional mechanism magnetizing the plasma on large-scales, and the possible emergence of a self-similar microscopic plasma configuration ([Katz et al., 2007](#)).

Such macroscopic magnetization cannot arise from electromagnetic, Weibel-like ([Fried, 1959](#)) streaming instabilities, which mediate the shock in the non-magnetized limit, without considerable subsequent growth of the magnetic coherence length l_B , as unstable Debye-scale modes rapidly decay downstream. Large-scale magnetization can however be produced if the shock encounters sufficient preexisting, extended upstream density inhomogeneities, as the resulting Richtmyer–Meshkov-like rippling of the shock surface can induce sustained downstream turbulence ([Giacalone and Jokipii, 2007](#); [Inoue et al., 2009](#); [Beresnyak et al., 2009](#); [Guo et al., 2012](#)). Even in the absence of such preexisting inhomogeneities, nonlinear modes developing in the shock precursor due to non-resonant CR streaming instabilities ([Bell, 2004](#); [Niemić et al., 2008](#); [Riquelme and Spitkovsky, 2009](#); [Amato and Blasi, 2009](#); [Stroman et al., 2009](#)) may induce macroscopic magnetization in non-oblique shocks

(Caprioli and Spitkovsky, 2013, 2014), provided that the far upstream is sufficiently magnetized to feed large l_B modes and carry the Alfvén waves needed to initiate particle acceleration. Such instabilities require $v_A \gg \eta v_d$ to avoid quenching by filamentation (Riquelme and Spitkovsky, 2009), marginally satisfied in SNRs where $B_u \gg 0.4\eta_3 \mu\text{G}$. Here, v_A and v_d are the Alfvén and downstream velocities, and $\eta \equiv 10^{-3}\eta_3$ is the upstream number density ratio between CRs and thermal plasma.

An analogous situation is inferred around the relativistic shocks of γ -ray burst (GRB) afterglows (Gruzinov and Waxman, 1999; Gruzinov, 2001; Katz et al., 2007), in which $\sigma \approx 10^{-9}$ and the magnetized layer is again vast in microscopic terms, suggesting the emergence of a self-similar plasma configuration (Katz et al., 2007). For instance, about a day after the burst, a near-equipartition magnetic field must persist over a downstream layer of proper width $\gtrsim 10^{17}$ cm, corresponding to $\gtrsim 10^{10}$ skin depths $l_{sd} = c/\omega_p$ for typical parameters, where ω_p is the plasma frequency and c is the speed of light. Electromagnetic modes on the order of l_{sd} (Medvedev and Loeb, 1999; Gruzinov and Waxman, 1999; Silva et al., 2003; Nishikawa et al., 2005; Spitkovsky, 2005; Kato, 2007) rapidly dissipate downstream, so cannot explain such a layer unless they somehow evolve into increasingly large structures (Gruzinov, 2001; Medvedev et al., 2005; Katz et al., 2007; Medvedev and Zakutnyaya, 2009; Pelletier et al., 2009; Reville and Bell, 2014; Lemoine, 2015).

Alternatively, as in SNRs, macroscopic magnetic layers could arise downstream of GRB afterglow shocks if sufficient preexisting density inhomogeneities are present far upstream (Sironi and Goodman, 2007; Milosavljević and Nakar, 2007; Goodman and MacFadyen, 2007). Such substructure could also arise from non-resonant CR streaming (Milosavljević and Nakar, 2006; Reville et al., 2006; Sironi and Spitkovsky, 2011) or other (Pelletier et al., 2009; Casse et al., 2013; Reville and Bell, 2014; Lemoine et al., 2014) instabilities in the precursor of the relativistic shock (Milosavljević and Nakar, 2006; Reville et al., 2006; Sironi and Spitkovsky, 2011), but only when σ is sufficiently large (e.g., Lemoine et al., 2014), and if upstream conditions suffice for the shock to produce magnetization on a range of scales needed to initiate CR acceleration (e.g., Lemoine et al., 2006).

The observed macroscopic downstream magnetization thus challenges the modelling of both non-relativistic shocks in SNRs, and their relativistic counterparts in GRB afterglows; both systems can be explained either by preexisting upstream density inhomogeneities, or by precursor inhomogeneities generated by combined upstream magnetization and CR streaming. These explanations can now be tested in strong virial, *i.e.* structure-formation accretion, shocks, which have non-relativistic $\sim 10^3 \text{ km s}^{-1}$ velocities similar to SNR shocks, but propagate into pristine, primordial infalling gas, which is very poorly magnetized and should not contain any significant substructure. We find that recent observations of virial shocks around galaxy clusters (see Fig. 1), and in particular their stacked synchrotron emission observed with the Owens Valley Radio Observatory Long Wavelength Array (OVRO-LWA,

hereafter LWA; Hou et al., 2023) and the Global Magneto-Ionic Medium Survey (GMIMS, radially polarized; Keshet, 2024), indicate downstream magnetization on macroscopic length-scales, exceeding (in natural units) those inferred from SNRs.

We review observations of virial shocks and their upstream conditions in §2, constrain their downstream magnetization in §3, and conclude with some implications for collisionless shock modelling in §4; a simple virial-shock synchrotron model is outlined in Appendix A. We adopt a flat Λ CDM cosmological model with a Hubble constant H of present value $H_0 = 70 \text{ km s}^{-1} \text{ Mpc}^{-1}$, an $\Omega_m = 0.3$ mass fraction, an $f_b = 0.17$ cosmic baryon fraction, and a $\Gamma = 5/3$ adiabatic index for the plasma. Assuming a 76% hydrogen mass fraction yields a mean $\bar{m} \approx 0.59m_p$ particle mass, where m_p is the proton mass.

2. Observations of virial shocks and their environment

Faint radiative signatures, predicted from virial shocks (Loeb and Waxman, 2000; Totani and Kitayama, 2000; Waxman and Loeb, 2000; Keshet et al., 2003; Miniati, 2002; Keshet et al., 2004; Kocsis et al., 2005), were identified in data stacked over many low-redshift galaxy clusters (Reiss et al., 2017; Reiss and Keshet, 2018; Hou et al., 2023; Keshet, 2024) once lengthscales were normalized by the R_{500} radius of each cluster. Here, R_{500} encloses a mean density $\rho_c \delta$ of contrast $\delta = 500$, where ρ_c is the critical mass density of the Universe. Such stacked signals, based on the Meta-Catalog of X-ray detected Clusters of galaxies (MCXC; Piffaretti et al., 2011) and at least two additional cluster catalogs (Ilani et al., 2024b; Nadler et al., 2024), were found narrowly confined near the same scaled $\tau \equiv r/R_{500} \approx 2.4$ cluster radius in very different channels, as demonstrated in Fig. 1. Similar, coincident signals were found in select nearby clusters (Keshet et al., 2017; Keshet and Reiss, 2018; Hurier et al., 2019; Keshet et al., 2020b), as illustrated in the figure (triangle symbols). The figure also shows (stars) the surprising coincident excess of discrete, cataloged radio and X-ray sources, energized by the virial shock (Ilani et al., 2024a,b).

Virial shocks are not expected to be spherical. The narrow $\tau \approx 2.4$ excess likely corresponds to the smallest distance from the center of the cluster (the semi-minor axis in an elliptic approximation), whereas a broad, tentative excess around $\tau \approx 6$ may correspond to the farthest (semi-major) distance (Hou et al., 2023; Ilani et al., 2024a), as illustrated in the figure by a simple cylindrical shock model of base radius $\tau = 2.4$ and half-height $\tau \approx 6$ (projected, averaged over all orientations, and binned, on top of a fixed background; see Keshet, 2024). The narrow excess roughly coincides with the dark-matter splashback radius, inferred from a localized drop in the logarithmic radial slopes of galaxy density profiles (More et al., 2016; Shin et al., 2019).

The diffuse synchrotron, inverse-Compton, and Sunyaev-Zel'dovich (SZ) signatures of the virial shock constrain the electron acceleration $\xi_e \approx 1\%$ and magnetization $\xi_B \approx \text{few } \%$ efficiencies, the $\gtrsim 10$ Mach numbers of the shocks, and the $\dot{M}/(MH) \approx 1$ mass accretion rate onto low-redshift clusters (Reiss et al., 2017; Reiss and Keshet, 2018; Hou et al.,

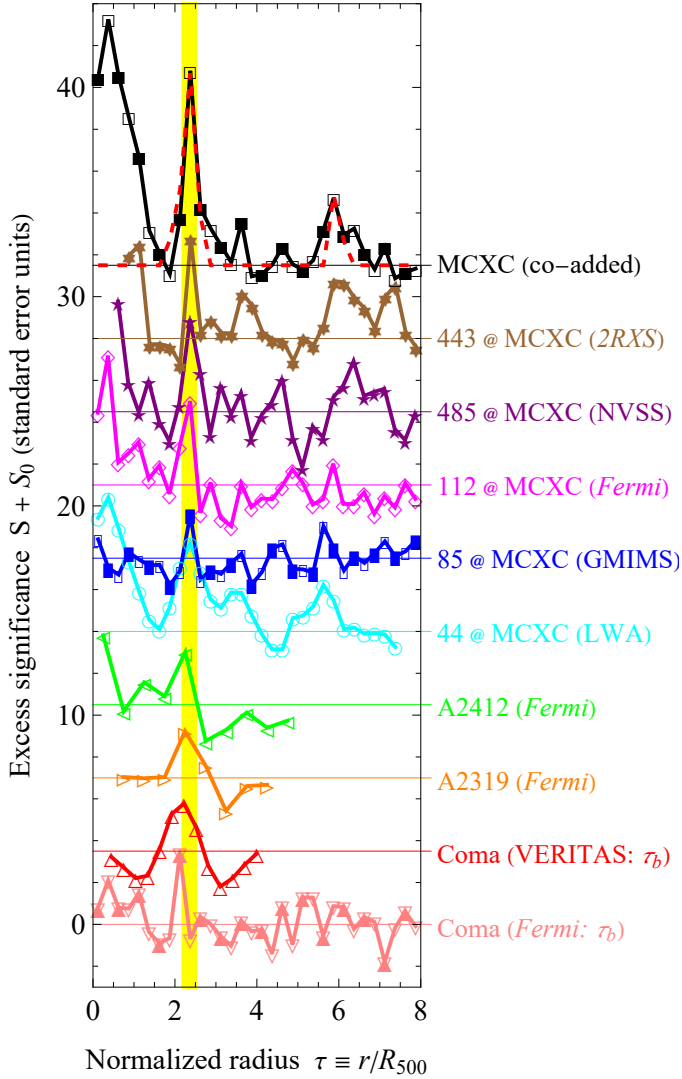


Figure 1: Virial shock signals identified in individual (triangles) or stacked (other symbols) clusters, in diffuse emission (empty symbols), discrete sources (filled), or without separating the two (intermittent empty and filled symbols). The significance S (symbols with lines to guide the eye, in standard-error units) of the excess above the background S_0 (labelled horizontal lines, shifted vertically for visibility) is plotted as a function of the normalized radius τ , for (bottom to top) clusters Coma, in *Fermi*-LAT (down triangles; Keshet and Reiss, 2018) and VERITAS (coincident with synchrotron emission and an SZ drop; up triangles; Keshet et al., 2017) data as a function of τ_b , A2319 (right triangles) and A2412 (left triangles) in *Fermi*-LAT data (coincident with SZ drops; Keshet et al., 2020b), and for stacked MCXC clusters (labels specify sample sizes) in LWA (circles; Hou et al., 2023), polarized GMIMS (rectangles; Keshet, 2024), and *Fermi*-LAT (diamonds; Reiss and Keshet, 2018) data, and in NVSS (five-stars) and 2XRS (six-stars) source catalogs (Ilani et al., 2024a). Also shown are the $2.2 < \tau < 2.5$ radial range (Reiss and Keshet, 2018) of MCXC virial-shock signals (vertical yellow band), the co-added MCXC excess (black squares), and a corresponding cylindrical shock model (dashed red curve; Keshet, 2024).

2023; Keshet and Reiss, 2018; Hurier et al., 2019; Keshet et al., 2020b). These estimates are based on the diffuse emission remaining after a careful removal of discrete sources, now known (Ilani et al., 2024a,b) to peak locally at the shock; the residual diffuse radio emission strengthens, as expected (Waxman and Loeb, 2000; Keshet et al., 2003), with cluster

mass M (Hou et al., 2023). The significant drop in projected SZ pressure at the shock, the shock strength (inferred from SZ and from the flat spectra of both inverse-Compton and synchrotron signals), the brightness of the leptonic signals, and anecdotal evidence (e.g., Keshet et al., 2017) all indicate that the $\tau \approx 2.4$ signals arise from the smooth accretion of primordial, cold gas, and not from heated gas accreted along filaments or streams.

The magnetic field far upstream of virial shocks is highly uncertain. Faraday rotation imposes model-dependent upper limits on intergalactic-medium (IGM) magnetic fields, such as $B < 4$ nG fields on \sim Mpc scales (O’Sullivan et al., 2020), $B < 30$ nG in large-scale filaments on $\gtrsim 1$ Mpc scales (Amaral et al., 2021; Carretti et al., 2022; Mtchedlidze et al., 2024), and $B < 10$ –30 nG on small, 0.07–0.20 kpc scales at redshifts $1 \lesssim z \lesssim 2$ (Padmanabhan and Loeb, 2023). Mean 40–80 nG fields recently attributed to $z = 0$ filaments (Carretti et al., 2023) pertain to warm, virialized regions of much higher densities than upstream of virial shocks, where the gas overdensity $\delta_g \lesssim 10$ (with respect to the cosmic mean gas density; see §3) is low. Indeed, comparable, 30–60 nG fields were associated with the claimed detection of synchrotron emission from stacked filaments (Vernstrom et al., 2021), attributed to shocked regions with amplified B (Vernstrom et al., 2023; Keshet, 2024). Extrapolating $z = 0$ filament estimates to $\delta_g \approx 10$ suggests 8–26 nG (Carretti et al., 2023) fields, but such an extrapolation again pertains at least in part to virialized gas. We conclude that upstream of the strong virial shocks of galaxy clusters, accreting from voids rather than filaments, B does not exceed a few nG, and could be much weaker.

3. Virial-shock magnetization

The spectra of inverse-Compton (Keshet and Reiss, 2018; Reiss and Keshet, 2018) and synchrotron (Hou et al., 2023; Keshet, 2024) emission from virial shocks, and the coincident sharp drop in SZ signal (Keshet et al., 2020b), are consistent with the strong shock limit, as expected for the virialization of primordial, cold gas. The shock velocity is then given by

$$v_u \approx 4v_d \approx \left(\frac{16k_B T_d}{3\bar{m}} \right)^{1/2} \approx 10^3 T_1 \text{ km s}^{-1}, \quad (1)$$

comparable to SNR shock velocities. Here, $T_d \equiv T_1 k_B^{-1}$ keV is the downstream temperature, subscripts u (d) denote upstream (downstream) quantities, and k_B is the Boltzmann constant.

For simplicity, we model the gas distribution using an isothermal β -model with the typical $\beta = 2/3$ of galaxy clusters, but take into account that due to peripheral steepening, the gas density may diminish by an additional factor $f_\beta \approx 1/3$ by the virial-shock radius (Hou et al., 2023). The particle number density upstream of the virial shock is then given by (see Appendix A and Hou et al., 2023)

$$n_u \approx \frac{n_d}{4} \approx \frac{f_\beta f_b \delta_s \rho_c}{12\bar{m}} \approx 10^{-5} f_\beta \delta_{90} \text{ cm}^{-3}, \quad (2)$$

where subscript s pertains to the shock radius,

$$\delta_s \approx 500\tau_s^{-2} \approx 87(\tau_s/2.4)^{-2}, \quad (3)$$

and $\delta_{90} \equiv \delta_s/90$.

The upstream gas density (2) is higher than its cosmic mean value by a factor

$$f_g = \frac{\bar{m}n_u}{f_b\Omega_m\rho_c} \simeq \frac{f_\beta\delta_s}{12\Omega_m} \simeq 25f_\beta\delta_{90}, \quad (4)$$

so pre-shock compression can amplify primordial magnetic fields B_p by a small factor $B_u/B_p \simeq f_g^{2/3}$ (in the isotropic case). The IGM magnetic field estimates reviewed in §2 indicate that unlike SNR shocks, the upstream of virial shocks is weakly magnetized, with plasma beta

$$\beta_p \simeq \frac{n_u k_B T_u}{B_u^2/8\pi} \simeq 2400B_1^{-2}f_\beta T_{10}\delta_{90}, \quad (5)$$

where $T_{10} \equiv k_B T_u/10 \text{ eV} \simeq 1$ according to cosmological simulations (Keshet et al., 2003), and $B_1 \equiv B_u/1 \text{ nG}$. Such upstream fields are far less significant dynamically than in SNR shocks,

$$\sigma \equiv \frac{B_u^2}{4\pi n_u \bar{m} u_u^2} \simeq 8 \times 10^{-7} \frac{B_1^2}{f_\beta T_{10} \delta_{90}}. \quad (6)$$

The properties of the downstream magnetic field can be inferred from the observed radio signal. In the strong-shock limit, cosmic-ray electron (CRE) injection with a flat energy spectrum of index $p = 2$ yields a steady-state volume-integrated (dimensionless) distribution

$$\frac{dN_e}{d\gamma} \simeq C\gamma^{-3} \quad (7)$$

in a cooling-limited range of Lorentz factors $\gamma < \gamma_{max}$, where C is a dimensionless constant. These CREs radiate a spectrally flat synchrotron luminosity

$$\nu L_\nu \simeq \frac{c\sigma_T C}{12\pi} B^2, \quad (8)$$

where σ_T is the Thomson cross section and ν is the frequency; estimates of the projected flux and brightness profiles are provided by Hou et al. (2023). Here and below, B^2 is defined as the mean squared magnetic-field amplitude in the region traversed by the radiating CREs before they cool. The magnetic energy fraction

$$\xi_B \equiv \frac{B^2/8\pi}{(3/2)n_d k_B T_d} \quad (9)$$

was estimated as $\sim 1\%$ by modeling the radio signal from Coma (Keshet et al., 2017), whereas the stacked LWA excess implies a somewhat stronger magnetization in the range $\xi_B \simeq (2-9)\%$ (Hou et al., 2023).

CREs at cluster peripheries cool primarily by inverse-Compton scattering cosmic-microwave background (CMB) photons, with a characteristic cooling time

$$t_{cool} \simeq \frac{3m_e c}{4u_{cmb}\sigma_T\gamma} \simeq 280\nu_{76}^{-1/2}(T_1 f_\beta \delta_{90} \xi_5)^{1/4} \text{ Myr}, \quad (10)$$

where the last estimate focuses on CREs synchrotron-radiating in LWA frequencies, $\nu_{76} \equiv \nu/76 \text{ MHz} \simeq 1$. Here, u_{cmb} is the

CMB energy density, m_e is the electron mass, and we defined $\xi_5 \equiv \xi_B/0.05$. At the highest CRE energies, the acceleration time $t_{acc} \simeq r_L c/(4u_d)^2$ is $t_0 \equiv t_{acc}(\gamma_{max}) = t_{cool}(\gamma_{max})$, yielding

$$\gamma_{max} \simeq \frac{v_u}{c} \left(\frac{3eB}{4u_{cmb}\sigma_T} \right)^{1/2} \simeq 7 \times 10^7 T_1^{3/4} (f_\beta \delta_{90} \xi_5)^{1/4}, \quad (11)$$

where e is the electron charge and r_L is the Larmor radius. This upper limit lies a factor of a few above the $\sim 9 \text{ TeV}$ energy of CREs radiating in $\sim 220 \text{ GeV}$ VERITAS energies (Keshet et al., 2017) and in the high-energy band of the stacked Fermi-LAT signal (Reiss and Keshet, 2018).

The acceleration of CREs to high energies requires strong magnetization around the shock, over a wide range of scales, needed to facilitate the Fermi cycles. The observed virial-shock γ -ray signals thus impose a lower limit on the width W of the downstream magnetized layer,

$$W > \frac{r_{LC}}{v_d} \simeq \frac{\gamma_{max} m_e c^3}{e B v_d} \simeq \frac{0.13}{(f_\beta T_1 \delta_{90} \xi_5)^{1/4}} \text{ kpc}. \quad (12)$$

In addition, a $v_u/v_d \simeq 4$ times narrower magnetized precursor is necessary upstream. Such magnetized layers are insufficiently wide, however, to account for the strength of the observed synchrotron signals (Keshet et al., 2017; Hou et al., 2023; Keshet, 2024). The low energy, $\gamma \ll \gamma_{max}$ CREs radiating at such radio frequencies escape the shock much faster than at high energies, after only a $\sim t_0\gamma/\gamma_{max}$ duration, and cool over a much longer, $t_0\gamma_{max}/\gamma$ time. As B^2 pertains to the field traversed during t_{cool} , and the corresponding ξ_B is already close to equipartition, much of the radio signal is emitted while these CREs are advected away from the shock, requiring an extended downstream magnetized region of width

$$W > v_d t_{cool} \simeq 66 T_1^{3/4} \nu_{76}^{-1/2} (f_\beta \delta_{90} \xi_5)^{1/4} \text{ kpc}. \quad (13)$$

In addition to advection, these CREs also diffuse as they radiate, but only over a relatively short distance $(r_L c t_{cool})^{1/2} \ll v_d t_{cool}$.

We conclude that accounting for the observed radio emission, and in particular the low-frequency LWA signal, requires an extended, macroscopic magnetized layer downstream of virial shocks. This layer is considerably thicker than required in SNR shocks, not only in its proper width, but also in terms of relevant physical quantities. In units of the downstream proton skin depth,

$$l_p \equiv \left(\frac{4\pi n_d e^2}{m_p} \right)^{1/2} \simeq \frac{3.3 \times 10^4}{(f_\beta \delta_{100})^{1/2}} \text{ km}, \quad (14)$$

the downstream magnetized layer has a minimal width

$$W/l_p > 6 \times 10^{13} (T_1 f_\beta \delta_{90})^{3/4} \nu_{76}^{-1/2} \xi_5^{1/4}. \quad (15)$$

More importantly, in terms of the downstream Debye length,

$$l_D \simeq \left(\frac{k_B T_d}{4\pi n_d e^2} \right)^{1/2} \simeq 34 \left(\frac{T_1}{f_\beta \delta_{90}} \right)^{1/2} \text{ km}, \quad (16)$$

the width becomes

$$W/l_D > 6 \times 10^{16} (f_\beta \delta_{90})^{3/4} \nu_{76}^{-1/2} (T_1 \xi_5)^{1/4}. \quad (17)$$

Similarly, $W/r_L(B) > 5 \times 10^9 T_1^{3/2} f_\beta \delta_{90} \xi_5 / \nu_{76}$, but the measured B^2 does not provide a reliable estimate of the Larmor radius in the patchy field expected downstream.

4. Discussion

The extended, $W \gtrsim 10^{16} l_D$ magnetized layers we infer downstream of virial shocks challenge the modeling of such weakly-magnetized, *i.e.* high M_A , shocks; this challenge is qualitatively more difficult than in the cases of SNR and GRB afterglow shocks. Attributing macroscopic magnetization to sufficient pre-existing density inhomogeneities is rather artificial even for SNR shocks, but becomes quite implausible for strong virial shocks, which propagate into pristine, non-virialized gas. Density inhomogeneities from non-resonant CR streaming instabilities in the shock precursor are also less likely in virial shocks, considering their weak upstream magnetization. In the weak fields of Eq. (5), the onset of CR acceleration may be greatly delayed, until sufficient magnetic substructure is generated to sustain the Fermi cycles. Non-resonant CR streaming instabilities must then compete with filamentation modes, as $\sigma \ll 10^{-3}$ by Eq. (6), and may become entirely quenched if the (poorly-constrained) upstream fields are sufficiently weak. For instance, the $\nu_A \gg \eta \nu_d$ growth condition may be violated in virial shocks, as it requires

$$B_u \gg 0.3 \eta_3 (f_\beta T_1 \delta_{90})^{1/2} \text{ nG}. \quad (18)$$

If non-resonant CR streaming instabilities are indeed quenched or greatly diminished in virial shocks, then the macroscopic magnetization we infer requires an alternative origin, such as nonlinear Weibel-like modes evolving hand-in-hand with particle acceleration to generate large-scale substructure, possibly developing a self-similar configuration (Katz et al., 2007). Fully ab-initio particle-in-cell (PIC) simulations have so far resolved only the initial stages of such shock evolution, mainly in 2D relativistic pair-plasma flows (Spitkovsky, 2008; Keshet et al., 2009; Lemoine et al., 2019; Grošelj et al., 2024). Early modes are limited to small-scales and decay too quickly (Gruzinov, 2001), as $k^3 c^3 / \omega_p$ (Chang et al., 2008; Lemoine, 2015), but the gradual acceleration of particles (Spitkovsky, 2008) drives magnetic substructure on increasingly long wavelengths λ , surviving farther downstream with a decay rate (Keshet et al., 2009)

$$\Gamma_B \equiv -\frac{d \ln B}{dt} \approx 0.7 \left(\frac{\lambda}{l_{sd}} \right)^{-2} \omega_p. \quad (19)$$

The slow l_B growth during the accessible, $t \sim [10^3, 10^4] \omega_p^{-1}$ downstream simulation times is associated with nonlinear, solitary low-density modes (cavities), emerging upstream following nonlinear filamentation (Keshet et al., 2009; Grošelj et al., 2024), and resulting in $\sim 10\%$ equipartition fields in 1% of the downstream area (Grošelj et al., 2024). Note that although the impossibility of a 2D dynamo and other limitations (*e.g.*, Gruzinov, 2008) do not rule out such kinetic upstream evolution, the 3D case is likely very different; a realistic ion-to-electron mass should also modify the picture.

If such a mechanism does dominate virial shocks, then it may well operate at some level also in other low σ systems, such as SNR and GRB afterglow shocks. Hybrid simulations (Caprioli and Spitkovsky, 2013, 2014) have established the dominance of non-resonant CR-streaming instabilities in non-oblique, non-relativistic shocks in the range $30 \lesssim M_A \lesssim 100$ for interstellar-medium (ISM) magnetization levels, but it is unclear if this mechanism remains dominant when taking into account kinetic electron effects over realistic length and time scales, and under more general physical conditions such as weaker magnetization.

Acknowledgements. We thank Y. Lyubarsky, I. Demidov, E. Waxman, and M. Gedalin for insightful discussions. This research was supported by the Israel Science Foundation (ISF grant No. 2126/22).

References

- Amaral, A.D., Vernstrom, T., Gaensler, B.M., 2021. Constraints on large-scale magnetic fields in the intergalactic medium using cross-correlation methods. *MNRAS* 503, 2913–2926. doi:10.1093/mnras/stab564, arXiv:2102.11312.
- Amato, E., Blasi, P., 2009. A kinetic approach to cosmic-ray-induced streaming instability at supernova shocks. *MNRAS* 392, 1591–1600. doi:10.1111/j.1365-2966.2008.14200.x, arXiv:0806.1223.
- Arad, O., Lavi, A., Keshet, U., 2021. Maximally hard radio spectra from fermi acceleration in pulsar-wind nebulae. *MNRAS* 504, 4952–4967. doi:10.1093/mnras/stab1044, arXiv:2012.00758.
- Axford, W.I., Leer, E., Skadron, G., 1977. The acceleration of cosmic rays by shock waves. in: International Cosmic Ray Conference, pp. 132–137.
- Bamba, A., Yamazaki, R., Ueno, M., Koyama, K., 2003. Small-Scale Structure of the SN 1006 Shock with Chandra Observations. *ApJ* 589, 827–837. doi:10.1086/374687, arXiv:astro-ph/0302174.
- Bell, A.R., 1978. The acceleration of cosmic rays in shock fronts. i. *MNRAS* 182, 147–156. doi:10.1093/mnras/182.2.147.
- Bell, A.R., 2004. Turbulent amplification of magnetic field and diffusive shock acceleration of cosmic rays. *MNRAS* 353, 550–558. doi:10.1111/j.1365-2966.2004.08097.x.
- Beresnyak, A., Jones, T.W., Lazarian, A., 2009. Turbulence-Induced Magnetic Fields and Structure of Cosmic Ray Modified Shocks. *ApJ* 707, 1541–1549. doi:10.1088/0004-637X/707/2/1541, arXiv:0908.2806.
- Blandford, R.D., Ostriker, J.P., 1978. Particle acceleration by astrophysical shocks. *ApJ* 221, L29–L32. doi:10.1086/182658.
- Bykov, A.M., Treumann, R.A., 2011. Fundamentals of collisionless shocks for astrophysical application, 2. relativistic shocks. *A&A Rev.* 19, 42. doi:10.1007/s00159-011-0042-8, arXiv:1105.3221.
- Caprioli, D., Spitkovsky, A., 2013. Cosmic-ray-induced filamentation instability in collisionless shocks. *ApJ* 765, L20. doi:10.1088/2041-8205/765/1/L20, arXiv:1211.6765.
- Caprioli, D., Spitkovsky, A., 2014. Simulations of ion acceleration at non-relativistic shocks. ii. magnetic field amplification. *ApJ* 794, 46. doi:10.1088/0004-637X/794/1/46, arXiv:1401.7679.
- Carretti, E., O’Sullivan, S.P., Vacca, V., Vazza, F., Gheller, C., Vernstrom, T., Bonafede, A., 2023. Magnetic field evolution in cosmic filaments with LOFAR data. *MNRAS* 518, 2273–2286. doi:10.1093/mnras/stac2966, arXiv:2210.06220.
- Carretti, E., Vacca, V., O’Sullivan, S.P., Heald, G.H., Horellou, C., Röttgering, H.J.A., Scaife, A.M.M., Shimwell, T.W., Shulevski, A., Stuardi, C., Vernstrom, T., 2022. Magnetic field strength in cosmic web filaments. *MNRAS* 512, 945–959. doi:10.1093/mnras/stac384, arXiv:2202.04607.
- Casse, F., Marcowith, A., Keppens, R., 2013. Non-resonant magnetohydrodynamics streaming instability near magnetized relativistic shocks. *MNRAS* 433, 940–951. doi:10.1093/mnras/stt772, arXiv:1305.0847.
- Chang, P., Spitkovsky, A., Arons, J., 2008. Long-Term Evolution of Magnetic Turbulence in Relativistic Collisionless Shocks: Electron-Positron Plasmas. *ApJ* 674, 378–387. doi:10.1086/524764, arXiv:0704.3832.

- Fried, B.D., 1959. Mechanism for Instability of Transverse Plasma Waves. *The Physics of Fluids* 2, 337–337. URL: <https://doi.org/10.1063/1.1705933>, doi:10.1063/1.1705933, arXiv:<https://pubs.aip.org/aip/pfl/article-pdf/2/3/337/12401439/137>
- Giacalone, J., Jokipii, J.R., 2007. Magnetic Field Amplification by Shocks in Turbulent Fluids. *ApJ* 663, L41–L44. doi:10.1086/519994.
- Goodman, J., MacFadyen, A., 2007. Ultra-relativistic geometrical shock dynamics and vorticity. ArXiv e-prints arXiv:0706.1818.
- Grošelj, D., Sironi, L., Spitkovsky, A., 2024. Long-term Evolution of Relativistic Unmagnetized Collisionless Shocks. *ApJ* 963, L44. doi:10.3847/2041-8213/ad2c8c, arXiv:2401.02392.
- Gruzinov, A., 2001. Gamma-ray burst phenomenology, shock dynamo, and the first magnetic fields. *ApJ* 563, L15–L18. doi:10.1086/324223, arXiv:arXiv:astro-ph/0107106.
- Gruzinov, A., 2008. Grb: magnetic fields, cosmic rays, and emission from first principles? arXiv e-prints, arXiv:0803.1182doi:10.48550/arXiv.0803.1182, arXiv:0803.1182.
- Gruzinov, A., Waxman, E., 1999. Gamma-ray burst afterglow: Polarization and analytic light curves. *ApJ* 511, 852–861. doi:10.1086/306720, arXiv:arXiv:astro-ph/9807111.
- Guo, F., Li, S., Li, H., Giacalone, J., Jokipii, J.R., Li, D., 2012. On the Amplification of Magnetic Field by a Supernova Blast Shock Wave in a Turbulent Medium. *ApJ* 747, 98. doi:10.1088/0004-637X/747/2/98, arXiv:1112.6373.
- Hou, K.C., Hallinan, G., Keshet, U., 2023. Synchrotron emission from virial shocks around stacked ovro-lwa galaxy clusters. *MNRAS* 521, 5786–5809. doi:10.1093/mnras/stad785, arXiv:2210.09317.
- Hurier, G., Adam, R., Keshet, U., 2019. First detection of a virial shock with sz data: implication for the mass accretion rate of abell 2319. *A&A* 622, A136. doi:10.1051/0004-6361/201732468.
- Ilani, G., Hou, K.C., Keshet, U., 2024a. Excess cataloged X-ray and radio sources at galaxy-cluster virial shocks. *J. Cosmology Astropart. Phys.* 2024, 008. doi:10.1088/1475-7516/2024/10/008, arXiv:2402.16946.
- Ilani, G., Hou, K.C., Nadler, G., Keshet, U., 2024b. Galaxy cluster virial-shock sources in erosita catalogs. *A&A* 686, L16. doi:10.1051/0004-6361/202449819, arXiv:2402.17822.
- Inoue, T., Yamazaki, R., Inutsuka, S.i., 2009. Turbulence and Magnetic Field Amplification in Supernova Remnants: Interactions Between a Strong Shock Wave and Multiphase Interstellar Medium. *ApJ* 695, 825–833. doi:10.1088/0004-637X/695/2/825, arXiv:0901.0486.
- Kato, T.N., 2007. Relativistic collisionless shocks in unmagnetized electron-positron plasmas. *ApJ* 668, 974–979. doi:10.1086/521297, arXiv:0707.0545.
- Katz, B., Keshet, U., Waxman, E., 2007. Self-similar collisionless shocks. *ApJ* 655, 375–390. doi:10.1086/509115, arXiv:arXiv:astro-ph/0607345.
- Keshet, U., 2017. Analytic study of 1d diffusive relativistic shock acceleration. *J. Cosmology Astropart. Phys.* 10, 25. doi:10.1088/1475-7516/2017/10/025.
- Keshet, U., 2024. Radially-polarized synchrotron from galaxy-cluster virial shocks. In preparation.
- Keshet, U., Arad, O., Lyubarski, Y., 2020a. Diffusive shock acceleration: Breakdown of spatial diffusion and isotropy. *ApJ* 891, 117. doi:10.3847/1538-4357/ab765e, arXiv:1910.08083.
- Keshet, U., Katz, B., Spitkovsky, A., Waxman, E., 2009. Magnetic field evolution in relativistic unmagnetized collisionless shocks. *ApJ* 693, L127–L130. doi:10.1088/0004-637X/693/2/L127, arXiv:0802.3217.
- Keshet, U., Kushnir, D., Loeb, A., Waxman, E., 2017. Preliminary evidence for a virial shock around the coma galaxy cluster. *ApJ* 845, 24. doi:10.3847/1538-4357/aa794b, arXiv:1210.1574.
- Keshet, U., Reiss, I., 2018. Evidence for an x-ray to gamma-ray virial shock signal from the coma cluster. *ApJ* 869, 53. doi:10.3847/1538-4357/aaeb1d.
- Keshet, U., Reiss, I., Hurier, G., 2020b. Coincident sunyaev-zel'dovich and gamma-ray signals from cluster virial shocks. *ApJ* 895, 72. doi:10.3847/1538-4357/ab8c49, arXiv:1801.01494.
- Keshet, U., Waxman, E., 2005. Energy spectrum of particles accelerated in relativistic collisionless shocks. *Physical Review Letters* 94, 111102+. doi:10.1103/PhysRevLett.94.111102, arXiv:arXiv:astro-ph/0408489.
- Keshet, U., Waxman, E., Loeb, A., 2004. Imprint of intergalactic shocks on the radio sky. *ApJ* 617, 281–302. doi:10.1086/424837, arXiv:arXiv:astro-ph/0402320.
- Keshet, U., Waxman, E., Loeb, A., Springel, V., Hernquist, L., 2003. Gamma-ray emission from intergalactic shocks. *ApJ* 585, 128–150. doi:10.1086/345946, arXiv:arXiv:astro-ph/0202318.
- Kirk, J.G., Guthmann, A.W., Gallant, Y.A., Achterberg, A., 2000. Particle acceleration at ultrarelativistic shocks: An eigenfunction method. *ApJ* 542, 235–242. doi:10.1086/309533, arXiv:arXiv:astro-ph/0005222.
- Kocsis, B., Haiman, Z., Frei, Z., 2005. Can virialization shocks be detected around galaxy clusters through the sunyaev-zel'dovich effect? *ApJ* 623, 632–649. doi:10.1086/427975, arXiv:arXiv:astro-ph/0409430.
- Krymskii, G.F., 1977. A regular mechanism for the acceleration of charged particles on the front of a shock wave. *Akademiia Nauk SSSR Doklady* 234, 1306–1308.
- Lavi, A., Arad, O., Nagar, Y., Keshet, U., 2020. Diffusive shock acceleration in n dimensions. *The Astrophysical Journal* 895, 107. doi:10.3847/1538-4357/ab8d2b, arXiv:2002.11123.
- Lemoine, M., 2015. Nonlinear collisionless damping of weibel turbulence in relativistic blast waves. *Journal of Plasma Physics* 81, 45101. doi:10.1017/S0022377814000920, arXiv:1410.0146.
- Lemoine, M., Gremillet, L., Pelletier, G., Vanthieghem, A., 2019. Physics of weibel-mediated relativistic collisionless shocks. *Phys. Rev. Lett.* 123, 35101. doi:10.1103/PhysRevLett.123.035101, arXiv:1907.07595.
- Lemoine, M., Pelletier, G., Gremillet, L., Plotnikov, I., 2014. A fast current-driven instability in relativistic collisionless shocks. *EPL (Europhysics Letters)* 106, 55001. doi:10.1209/0295-5075/106/55001, arXiv:1405.7360.
- Lemoine, M., Pelletier, G., Revenu, B., 2006. On the Efficiency of Fermi Acceleration at Relativistic Shocks. *ApJ* 645, L129–L132. doi:10.1086/506322, arXiv:astro-ph/0606005.
- Loeb, A., Waxman, E., 2000. Cosmic γ -ray background from structure formation in the intergalactic medium. *Nature* 405, 156–158. arXiv:arXiv:astro-ph/0003447.
- Medvedev, M.V., Fiore, M., Fonseca, R.A., Silva, L.O., Mori, W.B., 2005. Long-time evolution of magnetic fields in relativistic gamma-ray burst shocks. *ApJ* 618, L75–L78. doi:10.1086/427921, arXiv:astro-ph/0409382.
- Medvedev, M.V., Loeb, A., 1999. Generation of magnetic fields in the relativistic shock of gamma-ray burst sources. *ApJ* 526, 697–706. doi:10.1086/308038, arXiv:arXiv:astro-ph/9904363.
- Medvedev, M.V., Zakutnyaya, O.V., 2009. Magnetic fields and cosmic rays in grbs: A self-similar collisionless foreshock. *ApJ* 696, 2269–2274. doi:10.1088/0004-637X/696/2/2269, arXiv:0812.1906.
- Milosavljević, M., Nakar, E., 2006. The cosmic-ray precursor of relativistic collisionless shocks: A missing link in gamma-ray burst afterglows. *ApJ* 651, 979–984. doi:10.1086/507975, arXiv:arXiv:astro-ph/0512548.
- Milosavljevic, M., Nakar, E., 2007. The small-scale structure of ultrarelativistic blastwaves in gamma-ray burst afterglows, in: *American Astronomical Society Meeting Abstracts*, p. 18.07.
- Miniati, F., 2002. Intergalactic shock acceleration and the cosmic gamma-ray background. *MNRAS* 337, 199–208. doi:10.1046/j.1365-8711.2002.05903.x, arXiv:arXiv:astro-ph/0203014.
- More, S., Miyatake, H., Takada, M., Diemer, B., Kravtsov, A.V., Dalal, N.K., More, A., Murata, R., Mandelbaum, R., Rozo, E., Rykoff, E.S., Oguri, M., Spergel, D.N., 2016. Detection of the splashback radius and halo assembly bias of massive galaxy clusters. *ApJ* 825, 39. doi:10.3847/0004-637X/825/1/39, arXiv:1601.06063.
- Mtchedlidze, S., Domínguez-Fernández, P., Du, X., Carretti, E., Vazza, F., O'Sullivan, S.P., Brandenburg, A., Kahniashvili, T., 2024. Intergalactic medium rotation measure of primordial magnetic fields. arXiv e-prints, arXiv:2406.16230doi:10.48550/arXiv.2406.16230, arXiv:2406.16230.
- Nadler, G., Hou, K.C., Keshet, U., 2024. Stacked virial shocks. In preparation.
- Niemiec, J., Pohl, M., Stroman, T., Nishikawa, K.I., 2008. Production of Magnetic Turbulence by Cosmic Rays Drifting Upstream of Supernova Remnant Shocks. *ApJ* 684, 1174–1189. doi:10.1086/590054, arXiv:0802.2185.
- Nishikawa, K.I., Hardee, P., Richardson, G., Preece, R., Sol, H., Fishman, G.J., 2005. Particle acceleration and magnetic field generation in electron-positron relativistic shocks. *ApJ* 622, 927–937. doi:10.1086/428394, arXiv:arXiv:astro-ph/0410266.

- O'Sullivan, S.P., Brüggem, M., Vazza, F., Carretti, E., Locatelli, N.T., Stuardi, C., Vacca, V., Vernstrom, T., Heald, G., Horellou, C., Shimwell, T.W., Hardcastle, M.J., Tasse, C., Röttgering, H., 2020. New constraints on the magnetization of the cosmic web using LOFAR Faraday rotation observations. *MNRAS* 495, 2607–2619. doi:[10.1093/mnras/staa1395](https://doi.org/10.1093/mnras/staa1395), [arXiv:2002.06924](https://arxiv.org/abs/2002.06924).
- Padmanabhan, H., Loeb, A., 2023. A New Limit on Intergalactic Magnetic Fields on Subkiloparsec Scales from Fast Radio Bursts. *ApJ* 946, L18. doi:[10.3847/2041-8213/acc3a1](https://doi.org/10.3847/2041-8213/acc3a1), [arXiv:2301.08259](https://arxiv.org/abs/2301.08259).
- Pelletier, G., Lemoine, M., Marcowith, A., 2009. On fermi acceleration and magnetohydrodynamic instabilities at ultra-relativistic magnetized shock waves. *MNRAS* 393, 587–597. doi:[10.1111/j.1365-2966.2008.14219.x](https://doi.org/10.1111/j.1365-2966.2008.14219.x), [arXiv:0807.3459](https://arxiv.org/abs/0807.3459).
- Piffaretti, R., Arnaud, M., Pratt, G.W., Pointecouteau, E., Melin, J.B., 2011. The mcxc: a meta-catalogue of x-ray detected clusters of galaxies. *A&A* 534, A109. doi:[10.1051/0004-6361/201015377](https://doi.org/10.1051/0004-6361/201015377), [arXiv:1007.1916](https://arxiv.org/abs/1007.1916).
- Reiss, I., Keshet, U., 2018. Detection of virial shocks in stacked fermi-lat galaxy clusters. *J. Cosmology Astropart. Phys.* 2018, 010. doi:[10.1088/1475-7516/2018/10/010](https://doi.org/10.1088/1475-7516/2018/10/010), [arXiv:1705.05376](https://arxiv.org/abs/1705.05376).
- Reiss, I., Mushkin, J., Keshet, U., 2017. Detection of virial shocks in stacked fermi-lat clusters, in: *Proceedings of the 7th International Fermi Symposium*, p. 163. [arXiv:1705.05376](https://arxiv.org/abs/1705.05376).
- Ressler, S.M., Katsuda, S., Reynolds, S.P., Long, K.S., Petre, R., Williams, B.J., Winkler, P.F., 2014. Magnetic Field Amplification in the Thin X-Ray Rims of SN 1006. *ApJ* 790, 85. doi:[10.1088/0004-637X/790/2/85](https://doi.org/10.1088/0004-637X/790/2/85), [arXiv:1406.3630](https://arxiv.org/abs/1406.3630).
- Reville, B., Bell, A.R., 2014. On the maximum energy of shock-accelerated cosmic rays at ultra-relativistic shocks. *MNRAS* 439, 2050–2059. doi:[10.1093/mnras/stu088](https://doi.org/10.1093/mnras/stu088), [arXiv:1401.2803](https://arxiv.org/abs/1401.2803).
- Reville, B., Kirk, J.G., Duffy, P., 2006. A current-driven instability in parallel, relativistic shocks. *Plasma Physics and Controlled Fusion* 48, 1741–1747. doi:[10.1088/0741-3335/48/12/004](https://doi.org/10.1088/0741-3335/48/12/004), [arXiv:astro-ph/0608462](https://arxiv.org/abs/astro-ph/0608462).
- Riquelme, M.A., Spitkovsky, A., 2009. Nonlinear study of bell's cosmic ray current-driven instability. *ApJ* 694, 626–642. doi:[10.1088/0004-637X/694/1/626](https://doi.org/10.1088/0004-637X/694/1/626), [arXiv:0810.4565](https://arxiv.org/abs/0810.4565).
- Rybicki, G.B., Lightman, A.P., 1979. *Radiative processes in astrophysics*. John Wiley & Sons.
- Shin, T., Adhikari, S., Baxter, E.J., Chang, C., Jain, B., Battaglia, N., Bleem, L., Bocquet, S., DeRose, J., Gruen, D., Hilton, M., Kravtsov, A., McClintock, T., Rozo, E., Rykoff, E.S., Varga, T.N., Wechsler, R.H., Wu, H., Zhang, Z., Aiola, S., Allam, S., Bechtol, K., Benson, B.A., Bertin, E., Bond, J.R., Brodwin, M., Brooks, D., Buckley-Geer, E., Burke, D.L., Carlstrom, J.E., Carnero Rosell, A., Carrasco Kind, M., Carretero, J., Castander, F.J., Choi, S.K., Cunha, C.E., Crawford, T.M., da Costa, L.N., De Vicente, J., Desai, S., Devlin, M.J., Dietrich, J.P., Doel, P., Dunkley, J., Eifler, T.F., Evrard, A.E., Flaugher, B., Fosalba, P., Gallardo, P.A., García-Bellido, J., Gaztanaga, E., Gerdes, D.W., Gralla, M., Gruendl, R.A., Gschwend, J., Gupta, N., Gutierrez, G., Hartley, W.G., Hill, J.C., Ho, S.P., Hollowood, D.L., Honscheid, K., Hoyle, B., Huffenberger, K., Hughes, J.P., James, D.J., Jeltema, T., Kim, A.G., Krause, E., Kuehn, K., Lahav, O., Lima, M., Madhavacheril, M.S., Maia, M.A.G., Marshall, J.L., Maurin, L., McMahon, J., Menanteau, F., Miller, C.J., Miquel, R., Mohr, J.J., Naess, S., Nati, F., Newburgh, L., Niemack, M.D., Ogando, R.L.C., Page, L.A., Partridge, B., Patil, S., Plazas, A.A., Rapetti, D., Reichardt, C.L., Romer, A.K., Sanchez, E., Scarpine, V., Schindler, R., Serrano, S., Smith, M., Smith, R.C., Soares-Santos, M., Sobreira, F., Staggs, S.T., Stark, A., Stein, G., Suchyta, E., Swanson, M.E.C., Tarle, G., Thomas, D., van Engelen, A., Wollack, E.J., Xu, Z., 2019. Measurement of the splashback feature around sz-selected galaxy clusters with des, spt, and act. *MNRAS* 487, 2900–2918. doi:[10.1093/mnras/stz1434](https://doi.org/10.1093/mnras/stz1434), [arXiv:1811.06081](https://arxiv.org/abs/1811.06081).
- Silva, L.O., Fonseca, R.A., Tonge, J.W., Dawson, J.M., Mori, W.B., Medvedev, M.V., 2003. Interpenetrating plasma shells: Near-equipartition magnetic field generation and nonthermal particle acceleration. *ApJ* 596, L121–L124. doi:[10.1086/379156](https://doi.org/10.1086/379156), [arXiv:astro-ph/0307500](https://arxiv.org/abs/astro-ph/0307500).
- Sironi, L., Goodman, J., 2007. Production of magnetic energy by macroscopic turbulence in grb afterglows. *ApJ* 671, 1858–1867. doi:[10.1086/523636](https://doi.org/10.1086/523636), [arXiv:0706.1819](https://arxiv.org/abs/0706.1819).
- Sironi, L., Keshet, U., Lemoine, M., 2015. Relativistic shocks: Particle acceleration and magnetization. *Space Sci. Rev.* 191, 519–544. doi:[10.1007/s11214-015-0181-8](https://doi.org/10.1007/s11214-015-0181-8), [arXiv:1506.02034](https://arxiv.org/abs/1506.02034).
- Sironi, L., Spitkovsky, A., 2011. Acceleration of particles at the termination shock of a relativistic striped wind. *ApJ* 741, 39. doi:[10.1088/0004-637X/741/1/39](https://doi.org/10.1088/0004-637X/741/1/39), [arXiv:1107.0977](https://arxiv.org/abs/1107.0977).
- Spitkovsky, A., 2005. Simulations of relativistic collisionless shocks: shock structure and particle acceleration, in: Bulik, T., Rudak, B., Madejski, G. (Eds.), *Astrophysical Sources of High Energy Particles and Radiation*, pp. 345–350. doi:[10.1063/1.2141897](https://doi.org/10.1063/1.2141897), [arXiv:astro-ph/0603211](https://arxiv.org/abs/astro-ph/0603211).
- Spitkovsky, A., 2008. Particle acceleration in relativistic collisionless shocks: Fermi process at last? *The Astrophysical Journal Letters* 682, L5.
- Stroman, T., Pohl, M., Niemiec, J., 2009. Kinetic Simulations of Turbulent Magnetic-Field Growth by Streaming Cosmic Rays. *ApJ* 706, 38–44. doi:[10.1088/0004-637X/706/1/38](https://doi.org/10.1088/0004-637X/706/1/38), [arXiv:0909.5212](https://arxiv.org/abs/0909.5212).
- Totani, T., Kitayama, T., 2000. Forming clusters of galaxies as the origin of unidentified gev gamma-ray sources. *ApJ* 545, 572–577. doi:[10.1086/317872](https://doi.org/10.1086/317872), [arXiv:astro-ph/0006176](https://arxiv.org/abs/astro-ph/0006176).
- Treumann, R.A., 2009. Fundamentals of collisionless shocks for astrophysical application, I. non-relativistic shocks. *A&A Rev.* 17, 409–535. doi:[10.1007/s00159-009-0024-2](https://doi.org/10.1007/s00159-009-0024-2).
- Vanthieghem, A., Lemoine, M., Plotnikov, I., Grassi, A., Grech, M., Gremillet, L., Pelletier, G., 2020. Physics and phenomenology of weakly magnetized, relativistic astrophysical shock waves. *Galaxies* 8, 33. doi:[10.3390/galaxies802033](https://doi.org/10.3390/galaxies802033), [arXiv:2002.01141](https://arxiv.org/abs/2002.01141).
- Vernstrom, T., Heald, G., Vazza, F., Galvin, T.J., West, J.L., Locatelli, N., Fornengo, N., Pinetti, E., 2021. Discovery of magnetic fields along stacked cosmic filaments as revealed by radio and x-ray emission. *Monthly Notices of the Royal Astronomical Society* 505, 4178–4196. URL: <https://doi.org/10.1093/mnras/stab1301>, doi:[10.1093/mnras/stab1301](https://doi.org/10.1093/mnras/stab1301), <https://academic.oup.com/mnras/article/505/4/4178/6311301>.
- Vernstrom, T., West, J., Vazza, F., Wittor, D., Riseley, C.J., Heald, G., 2023. Polarized accretion shocks from the cosmic web. *Science Advances* 9, eade7233. doi:[10.1126/sciadv.ade7233](https://doi.org/10.1126/sciadv.ade7233), [arXiv:2302.08072](https://arxiv.org/abs/2302.08072).
- Vink, J., 2020. Physics and Evolution of Supernova Remnants. doi:[10.1007/978-3-030-55231-2](https://doi.org/10.1007/978-3-030-55231-2).
- Vink, J., Laming, J.M., 2003. On the Magnetic Fields and Particle Acceleration in Cassiopeia A. *ApJ* 584, 758–769. doi:[10.1086/345832](https://doi.org/10.1086/345832), [arXiv:astro-ph/0210669](https://arxiv.org/abs/astro-ph/0210669).
- Völk, H.J., Berezhko, E.G., Ksenofontov, L.T., 2005. Magnetic field amplification in tycho and other shell-type supernova remnants. *A&A* 433, 229–240. doi:[10.1051/0004-6361:20042015](https://doi.org/10.1051/0004-6361:20042015), [arXiv:astro-ph/0409453](https://arxiv.org/abs/astro-ph/0409453).
- Waxman, E., Loeb, A., 2000. Fluctuations in the radio background from intergalactic synchrotron emission. *ApJ* 545, L11–L14. doi:[10.1086/317326](https://doi.org/10.1086/317326), [arXiv:astro-ph/0007049](https://arxiv.org/abs/astro-ph/0007049).

Appendix A. Virial-shock synchrotron model

We reproduce the virial shock model of Hou et al. (2023), including its synchrotron estimate. We begin with the isothermal β -model, in which the particle number density follows

$$n(r) = n_0 \left[1 + \left(\frac{r}{r_c} \right)^2 \right]^{-3\beta/2}, \quad (\text{A.1})$$

where n_0 is the central number density, r_c is the core radius, and β is the slope parameter. In the hydrostatic equilibrium limit, the total (gravitating) mass inside a radius r is given by

$$M(r) \approx \frac{3\beta k_B T r}{G \bar{m}} \left(1 + \frac{r_c^2}{r^2} \right)^{-1}, \quad (\text{A.2})$$

where G is Newton's constant. The typical $r_c \sim 0.1R_{500}$ core radius is much smaller than the $r \gtrsim 2R_{500}$ radii of interest, so we may approximate the downstream distribution as $n(r) \approx n_0 (r/r_c)^{-3\beta}$, and the corresponding mass as

$$M(r) \approx \frac{3\beta k_B T}{G \bar{m}} r. \quad (\text{A.3})$$

In this approximation, the over-density parameter $\delta = 500/\tau^2$ yields $\delta_s(\tau_s \simeq 2.4) \simeq 90$, where subscript s denotes evaluation at the shock radius. The enclosing radius

$$R_\delta = \left[\frac{9\beta k_B T}{4\pi\rho_c(z)\delta G\bar{m}} \right]^{1/2} \quad (\text{A.4})$$

and mass-temperature relation

$$M_\delta = \frac{9}{2\sqrt{\pi\rho_c(z)\delta}} \left(\frac{\beta k_B T}{G\bar{m}} \right)^{3/2}, \quad (\text{A.5})$$

are defined such the mean mass density $M_\delta/[(4/3)\pi R_\delta^3]$ enclosed within a radius R_δ is higher by a factor δ than the $\rho_c(z) \equiv \rho_0 \mathcal{H}^2$ critical mass density of the Universe, with $\rho_0 = 3H_0^2/(8\pi G)$ being the present value $\rho_c(0)$ and $\mathcal{H} \equiv H(z)/H_0 \simeq [(1-\Omega_m) + (1+z)^3\Omega_m]^{1/2}$ describing the evolution of the Hubble constant. Assuming that the total baryon mass $f_b M_s$ is given by the spatial integral of the isothermal β -profile (A.1) now yields the downstream particle number density,

$$n_d = (1-\beta)f_\beta \frac{f_b \rho_c(z)}{\bar{m}} \delta_s, \quad (\text{A.6})$$

where the factor $f_\beta \simeq 1/3$ was introduced to account for the deviation from the β -model profile at the cluster periphery.

We assume that a fraction ξ_e of the thermal energy density downstream of the shock is deposited in the CRE distribution (7), spanning the $\gamma_1 < \gamma < \gamma_2$ range. The effective value of γ_1 has little effect on our results, so is taken for simplicity as unity. The volume-integrated normalization in Eq. (7) is then given by

$$C = \frac{9k_B T \xi_e}{8(p-1)c u_{cmb} \sigma_T} \frac{f_b \dot{M}_s}{\bar{m}} \times \begin{cases} \frac{1}{\ln(\gamma_2/\gamma_1)} & \text{for } p = 2; \\ \frac{p-2}{\gamma_1^{2-p} - \gamma_2^{2-p}} & \text{for } p \neq 2, \end{cases} \quad (\text{A.7})$$

where we adopted the typical $\beta = 2/3$ (henceforth). To estimate the number accretion rate $f_b \dot{M}_s/\bar{m}$ of gas particles through the shock, we parameterize the accretion rate as proportional to M_s by introducing the dimensionless accretion parameter

$$\dot{m} \equiv \frac{\dot{M}_s}{M_s H(z)}. \quad (\text{A.8})$$

The synchrotron luminosity radiated by a CRE population of steady-state spectral index $p+1$ is (*e.g.*, Rybicki and Lightman, 1979)

$$L_\nu = \alpha_e h \nu C \Phi q(p) \left(\frac{3\nu_B}{\nu} \right)^{1+\frac{p}{2}}, \quad (\text{A.9})$$

where $\alpha_e = e^2/(\hbar c)$ is the fine-structure constant, $h = 2\pi\hbar$ is Planck's constant, $\nu_B = eB/(2\pi m_e c)$ is the cyclotron frequency, $\Gamma(y)$ is the gamma function, and the p -dependent numerical factor

$$q(p) \equiv \frac{\Gamma\left(\frac{p}{4} + \frac{11}{6}\right)\Gamma\left(\frac{p}{4} + \frac{1}{6}\right)}{(p+2)\sqrt{3}}. \quad (\text{A.10})$$

The dependence $\Phi \equiv \sin^{(p+2)/2} \phi$ upon the pitch angle ϕ is isotropically averaged to give

$$\langle \Phi \rangle = \frac{\sqrt{\pi} \Gamma\left(\frac{p}{4} + \frac{3}{2}\right)}{2\Gamma\left(\frac{p}{4} + 2\right)}, \quad (\text{A.11})$$

leading to Eq. (8). For the corresponding flux and brightness profiles, see Hou et al. (2023).